PHYSICAL REVIEW B **83**, 115107 (2011)

Influence of interband transition on the laser-induced voltage in thermoelectric Ca_xCoO_2 thin films

Kouhei Takahashi,* Tsutomu Kanno, Akihiro Sakai, Hideaki Adachi, and Yuka Yamada
Advanced Technology Research Laboratories, Panasonic Corporation, 3-4 Hikaridai, Seika-cho, Soraku-gun, Kyoto 619-0237, Japan
(Received 6 December 2010; revised manuscript received 20 January 2011; published 4 March 2011)

Laser-induced voltages in incline-oriented thin films of thermoelectric Ca_xCoO_2 have been investigated at four laser wavelengths. Large film in-plane voltage signals, several tens of volts, were identified at each wavelength regardless of the occurrence of interband optical transition. The thermal model based on heat conduction equation demonstrates that this transverse voltage is closely related to heat conduction normal to the film surface and, hence, that it is associated with a phenomenon called the off-diagonal thermoelectric effect. However, distinct discrepancies between the experiment and the thermal model were identified for short laser wavelengths at which interband transition occurred. We discuss the discrepancies in terms of a photovoltaic effect (the photo-Dember effect), showing that the laser-induced voltage may not be purely thermal in origin when it is accompanied by interband transition.

DOI: 10.1103/PhysRevB.83.115107 PACS number(s): 72.20.Pa, 78.20.nd, 68.60.Dv

I. INTRODUCTION

Incline-oriented thin films composed of anisotropic materials show unusually large transverse voltage signals upon laser illumination. This phenomenon was first demonstrated in $YBa_2Cu_3O_{7-\delta}$[1–5] and, further, in other perovskite-related materials such as $La_{1-x}Ca_xMnO_3$[6–8] and, more recently, in thermoelectric Ca_xCoO_2.[9] The origin of the large laser-induced voltage was explained by an unconventional thermoelectric phenomenon called the off-diagonal thermoelectric (ODTE) effect. The ODTE effect is a thermoelectric phenomenon, which utilizes the off-diagonal term of the Seebeck coefficient tensor **S**. This phenomenon emerges in anisotropic materials when they satisfy a special crystal orientation. Figure 1 shows an example of the schematic crystal orientation necessary to develop the ODTE effect in Ca_xCoO_2 thin films. Ca_xCoO_2 is a member of the layered cobaltites with CdI_2-type CoO_2 layers.[10] The crystal structure is composed of alternate stacks of conductive CoO_2 planes and insulating Ca_x sheets. Due to this layered structure, carrier transport is restricted within the CoO_2 planes, which results in anisotropic physical properties between the directions parallel and perpendicular to the CoO_2 planes, that is, between the *ab* planes and the *c* axis. In Fig. 1, the CoO_2 planes (the *ab* planes) are tilted with respect to the substrate surface by an angle θ. The tilted crystal orientation together with the anisotropic property of Ca_xCoO_2 gives rise to a nonzero component in the off-diagonal term of **S**.[11] Given the fundamental formula of the Seebeck effect as $\mathbf{E} = \mathbf{S}\nabla\mathbf{T}$ ($\mathbf{E}$ and $\nabla\mathbf{T}$ being the electric field vector and the temperature gradient vector, respectively), the aforementioned condition allows us to generate a thermoelectric voltage in a film in the *in-plane* direction (on the *x* axis) by introduction of a temperature gradient in the *out-of-plane* direction (on the *z* axis) (see Fig. 1). This is in contrast to the ordinary thermoelectric effect, in which the voltage is generated in the same direction as the applied temperature gradient. The film in-plane voltage V_x generated by the ODTE effect is expressed in the form[11]

$$V_x = \frac{l}{2}\nabla_z T\,\Delta S \sin 2\theta = \frac{l}{2}\frac{\Delta T_z}{d}\Delta S \sin 2\theta. \qquad (1)$$

Here, ΔS is the difference in the Seebeck coefficient between the *ab* planes and the *c* axis arising from the anisotropic feature, l is the length of the sample, d is the thickness of the sample, $\nabla_z T$ is the film out-of-plane temperature gradient, and ΔT_z is the temperature difference between the front and the back sides of the film.

The ODTE effect is unique in the sense that a large voltage can be generated by a very small temperature difference. For example, in thin films with a typical dimension of $l = 10$ mm and $d = 100$ nm, V_x can reach up to several hundred millivolts by a ΔT_z of merely 1 K. The large voltage is reasonable given that V_x is proportional to the sample aspect ratio l/d, which is as large as 10^5 in the aforementioned case. Since pulsed laser illumination can easily induce ΔT_z of several tens of kelvins, large voltage signals, several tens of volts, observed in previous studies, can indeed be expected via this mechanism.

However, there are discussions suggesting that the laser-induced voltages are somewhat related to photovoltaic effects, and not purely thermal in origin.[8,12] This is because the laser photon energy E_{photon} used in most previous studies exceeds the band gap energy E_g of the material, which induces interband transition and generation of photoexcited carriers. Zhao *et al.* have reported that, in $La_{1-x}Ca_xMnO_3$ thin films, voltage signals were only observable under the condition of $E_{\text{photon}} > E_g$, which indicates a photovoltaic origin.[8] In contrast, in $YBa_2Cu_3O_{7-\delta}$ thin films, voltage signals have been observed even under the condition of $E_{\text{photon}} < E_g$,[4] which supports the temperature-driven origin. This contradiction complicates the true origin of the laser-induced voltage. The previous studies indeed provide reasonable explanations, which indicate the connection between the ODTE effect and the large voltage signal. However, it is also true that these studies do not provide sufficient explanation to exclude the contribution of photovoltaic effects. In the present work, we have measured the laser-induced voltage characteristics of Ca_xCoO_2 thin films at four wavelengths λ and investigated the influence of interband transition on the resultant voltage signal. Ca_xCoO_2 exhibits ΔS of 35 μV/K,[13] which is larger by a factor of 5 than the other previously studied materials. The large ΔS makes this material suitable for identification of the contribution of the ODTE effect to the generated voltage.

The remainder of this paper is organized as follows. In Sec. II, we briefly describe the structural and optical properties

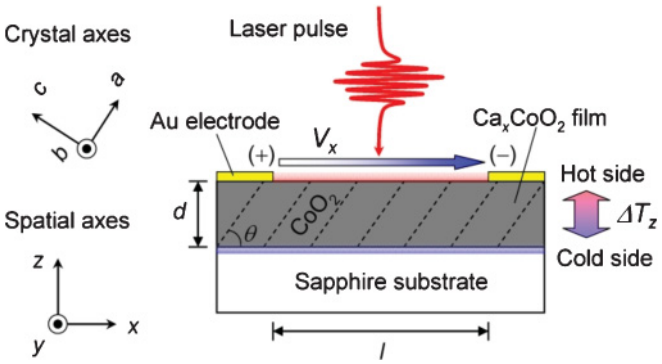

FIG. 1. (Color online) (a) Experimental configuration to measure the ODTE effect. A schematic cross-section view of the tilted Ca_xCoO_2 thin films are shown. The *abc* axes and the *xyz* axes represent the crystal axes and the spatial axes, respectively. Dotted lines, which are tilted with respect to the film surface by an angle θ, represent the CoO_2 planes (*ab* planes) of Ca_xCoO_2.

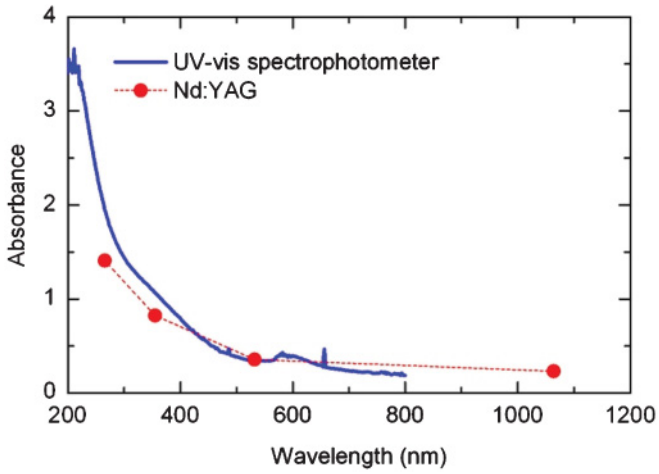

FIG. 2. (Color online) Absorbance spectrum of a 150-nm-thick Ca_xCoO_2 thin film in the near-infrared to ultraviolet region measured by a UV-vis spectrophotometer. The absorbance measured using a Nd:YAG laser as the light source is also shown. The dotted line is a guide for the eye.

of the inclined Ca_xCoO_2 films and explain the experimental conditions of the present study. In Sec. III, we explain the thermal model based on one-dimensional heat conduction equation, which is used to calculate the time profile of the laser-induced temperature change of the film and the resultant thermoelectric voltage expected via the ODTE effect. In Sec. IV, we compare the measured voltage waveforms with those simulated by the thermal model in terms of the time profile (Sec. IV A) and the peak voltage (Sec. IV B). We show that the experimental results are in fairly good agreement with the thermal model, which indicates that the laser-induced voltage is indeed associated with the ODTE effect. However, we also show that there is a distinct discrepancy between the experiment and the thermal model at short λ where interband transition occurs. In Sec. V, we explain the origin of the discrepancies in terms of the photo-Dember effect and suggest that the laser-induced voltage is mainly thermal in origin but is affected by a photovoltaic effect when it is accompanied by an interband transition. A summary of the paper is then given in Sec. VI.

II. EXPERIMENT

Figure 1 shows the sample configuration of the present experiment. Ca_xCoO_2 ($x \sim 0.5$) thin films were grown on *n*-plane [$(11\bar{2}3)$-plane] sapphire single-crystal substrates by magnetron sputtering. The film thickness of *d* was varied from 15 to 400 nm. The inclined crystal orientation of the films ($\theta = 59^\circ$) was confirmed by four-circle x-ray diffraction analysis. Details of thin film fabrication and structural characterization are described in Ref. 14. Two pairs of Au electrodes were fabricated on the film surface to measure film in-plane voltage signals along two orthogonal directions, that in, the *x* axis and the *y* axis. The distance between the electrodes *l* were fixed at 6 mm. Note that the projection of the tilted *c* axis onto the film surface is directed along the *x* axis.

A Q-switched Nd:YAG pulse laser at four λ values was used for characterization, that is, the fundamental harmonic at a λ of 1064 nm, the second harmonic at a λ of 532 nm, the third harmonic at a λ of 355 nm, and the fourth harmonic at a λ of 266 nm. The pulse width and the repetition rate of the laser pulses were 8 ns and 50 Hz, respectively. The laser fluency was fixed at 3.5 mJ/cm^2 unless noted otherwise. Figure 2 shows the room-temperature absorbance spectrum of a 150-nm-thick Ca_xCoO_2 film in the near-infrared to ultraviolet region measured by a UV-vis spectrophotometer. We also plot the absorbance of the same film at λ of 1064, 532, 355, and 266 nm, which were measured using a Nd:YAG laser as the light source. A marked increase in absorbance is observed below a λ of ∼500 nm, which indicates the occurrence of interband transition (E_g is estimated to be ∼2.5 eV). This means that interband transition is expected by laser illumination at a λ of 355 and 266 nm but not at a λ of 1064 and 532 nm.

The beam shape of the Nd:YAG laser was adjusted to a circle (diameter, 6 mm) using a beam expander and an aperture. The laser beam was carefully illuminated at the film center so as to avoid temperature difference between the electrodes. A temperature gradient is thus expected only in the film out-of-plane direction by laser illumination. Voltage waveforms between the electrodes were measured by a digital oscilloscope with a 500-MHz bandwidth. All measurements were performed at room temperature.

The basic theory suggests that the ODTE voltage is generated only in the direction parallel to the projection of the tilted *c* axis onto the film surface, that is, the *x* axis in Fig. 1. To verify this aspect, we examined the responses on the *y* axis prior to detailed measurements. As a result, we confirmed that voltage signals indeed do not develop in the *y* axis for each λ. The present work is therefore devoted to the responses on the *x* axis.

III. THERMAL MODEL

The thermal model considered here is based on one-dimensional heat conduction equation. A similar model has been used to describe the laser-induced responses in $YBa_2Cu_3O_{7-\delta}$ thin films.[3,15] Upon laser illumination, a

temperature gradient is introduced perpendicular to the film surface (on the z axis). If the film is hit by the laser pulse at time $t = 0$, the temperature T distribution of the film at $t = 0$ will be given by

$$T(z,0) = T_0 + T_{\text{rise}} = T_0 + \frac{I\alpha}{C}(1 - R)\exp(-\alpha z), \tag{2}$$

where T_0 is the initial temperature of the film (and the substrate) before laser absorption, T_{rise} is the temperature rise of the film immediately after laser absorption, I is the laser fluency, α is the absorption coefficient of the film, and R is the reflectivity of the film. Here we define the z position at the film surface and the film/substrate interface as $z = 0$ and $z = d$, respectively. The temperature of the film at time t and position z will then be described by the one-dimensional heat conduction equation

$$\frac{\partial T}{\partial t} = D_{\text{T}}\frac{\partial^2 T}{\partial z^2}, \tag{3}$$

where D_{T} is the thermal diffusivity of the film expressed as $D_{\text{T}} = \kappa/C$ (κ, thermal conductivity; C, volumetric specific heat). Given that the film surface is thermally insulating and that heat loss at the film/substrate interface is governed by the thermal boundary resistance R_{bd}, the above diffusion equation is subjected to the following boundary conditions:

$$J_{\text{Q}}(0,t) = 0, \tag{4}$$

$$J_{\text{Q}}(d,t) = \Delta T_{\text{bd}}/R_{\text{bd}}. \tag{5}$$

Here, J_{Q} is the heat flux and ΔT_{bd} is the temperature drop at the film/substrate interface. We assume that the substrate acts as a perfect heat sink, whose temperature remains unchanged, namely, $\Delta T_{\text{bd}} = T(d,t) - T_0$.

From the initial temperature distribution and the boundary conditions, the solution of the differential equation, Eq. (3) is given by

$$T(z,t) = T_0 + \sum_{n=1}^{\infty} F_n \cos\left(\frac{\gamma_n z}{d}\right)\exp\left(-\frac{\gamma_n^2 D_{\text{T}}}{d^2}t\right). \tag{6}$$

In this equation, γ_n are the positive roots of $\gamma\tan\gamma = \eta$, where $\eta = R_{\text{f}}/R_{\text{bd}}$. R_{f} is the thermal resistance of the film, which is expressed as $R_{\text{f}} = d/\kappa$. F_n is given by

$$F_n = \frac{2}{d}\left(1 + \frac{\eta}{\eta^2 + \gamma_n^2}\right)^{-1}\int_0^d T_{\text{rise}}\cos\left(\frac{\gamma_n z}{d}\right)dz. \tag{7}$$

Finally, the temporal profile of ΔT_z is expressed as

$$\begin{aligned}\Delta T_z(t) &= T(0,t) - T(d,t)\\ &= \sum_{n=1}^{\infty} F_n(1 - \cos\gamma_n)\exp\left(-\frac{\gamma_n^2 D_{\text{T}}}{d^2}t\right).\end{aligned} \tag{8}$$

However, it should be noted that $\Delta T_z(t)$ in Eq. (8) describes the situation when the film is hit by a delta function shaped laser pulse, whereas the actual laser pulse in the present experiment exhibits a Gaussian profile with a finite duration of 8 ns. In this case, $\Delta T_z(t)$ should be rewritten by the convolution of Eq. (8) with the laser profile,

$$\Delta T_z(t) = \int_{-\infty}^{\infty} f(\beta)g(t - \beta)\,d\beta. \tag{9}$$

Here, f is the right side of Eq. (8) and g is the temporal profile of the laser pulse, which is given by

$$g(t) = \frac{2I}{w\sqrt{\pi}}\exp\left(-\frac{4t^2}{w^2}\right), \tag{10}$$

where w is the laser pulse width (=8 ns).

Using this thermal model, $\Delta T_z(t)$ values established in Ca_xCoO_2 thin films by laser illumination were calculated for different d and λ. The time development of the resultant ODTE voltages, namely, $V_x(t)$, were then calculated by substituting $\Delta T_z(t)$ into Eq. (1). α values used in the simulation were taken from the absorbance spectrum in Fig. 2, that is, 2.5×10^4, 4.1×10^4, 9.2×10^4, and 13.1×10^4 cm^{-1} at λ of 1064, 532, 355, and 266 nm, respectively. R was 0.1 at all λ. The unknown physical quantities of Ca_xCoO_2 such as κ and C were substituted by those of Na_xCoO_2 ($\kappa = 0.04$ W/cm K[16] and $C = 1.65$ J/cm^3 K[17]). R_{bd} was left as a free fitting parameter to achieve the best fits to the experiment (varied from 1.0×10^{-5} to 1.0×10^{-3} K cm^2/W). We chose an R_{bd} of 2.0×10^{-4} K cm^2/W, which gave good fits for each λ. This value is comparable to that in previous reports on $YBa_2Cu_3O_{7-\delta}$ thin films.[3,15]

IV. RESULTS

A. Time profiles

The solid lines in Fig. 3 show the measured voltage waveforms of a 150-nm-thick Ca_xCoO_2 film in response to laser illumination at four different λ values. Each waveform is vertically offset for clarity. A pulsed voltage signal with a fast duration of ~20 ns is identified at each λ, all of which exhibit a peak value V_{peak} exceeding several tens of volts. The large voltage signals at $\lambda = 1064$ and 532 nm clearly manifests that $E_{\text{photon}} > E_{\text{g}}$ is not a necessary condition to generate the

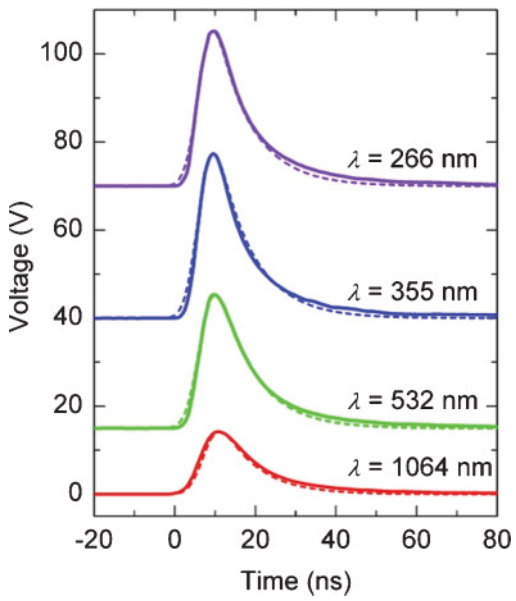

FIG. 3. (Color online) Laser-induced voltage waveforms of a 150-nm-thick Ca_xCoO_2 thin film at various λ. Solid lines and dashed lines represent the experimental waveforms and the simulated waveforms, respectively. Waveforms at each λ are vertically offset for clarity.

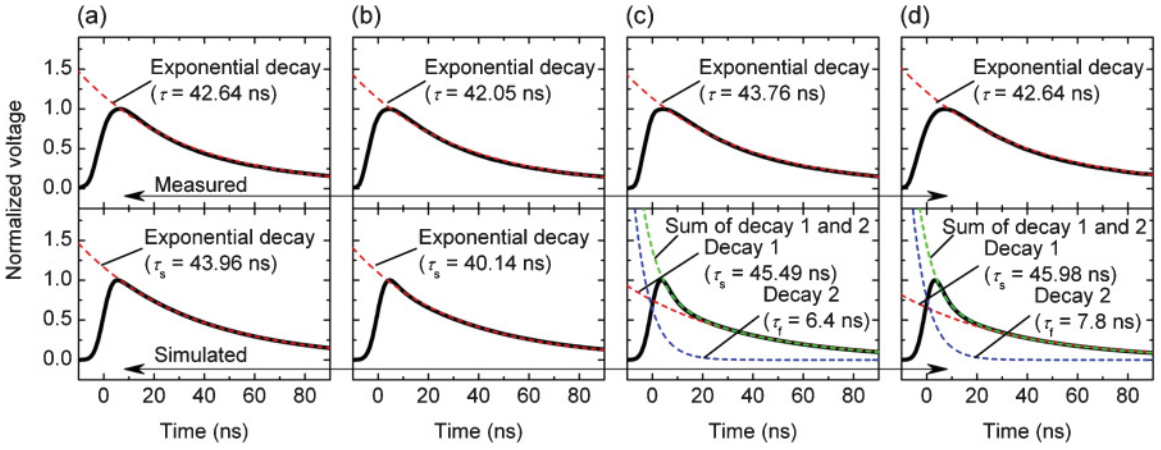

FIG. 4. (Color online) Measured voltage waveforms (upper panel) and simulated voltage waveforms (lower panel) of the 400-nm-thick film at (a) $\lambda = 1064$ nm, (b) 532 nm, (c) 355 nm, and (d) 266 nm (solid lines). Note that each waveform is normalized by the peak values. Exponential decay fits for each waveform are also shown, by dashed lines.

laser-induced voltage. We also show by the dashed lines in Fig. 3 the simulated waveforms obtained by the thermal model. The simulated waveforms are normalized by the experimental V_{peak} at each λ so as to compare the time development of the two curves. We see that the simulated curves trace the experimental ones well in this film thickness. Although the simulated waveforms are normalized for clarity, the value of V_{peak} in the experiment and the simulation actually lie within the same order of magnitude [see Figs. 6(a) and 6(b)]. These aspects support that the laser-induced voltage is related to the ODTE effect. We mentioned that laser-induced voltage signals were only observable under the condition of $E_{\text{photon}} > E_{\text{g}}$ in $La_{1-x}Ca_xMnO_3$ thin films.[8] We assume that this is due to the extremely small ΔS of $La_{1-x}Ca_xMnO_3$ (0.22 μV/K), which requires a large ΔT_z to generate a measurable voltage signal. It is obvious that laser illumination under the condition of $E_{\text{photon}} > E_{\text{g}}$ induces a large ΔT_z due to the significant increase in laser absorption.

The thermal model reproduced the time profile of the measured voltages well for most d and λ as shown in Fig. 3. However, a distinct discrepancy was observed in the 400-nm-thick film at $\lambda = 355$ and 266 nm. In Fig. 4, we show the measured voltage waveforms (upper panels) and the simulated voltage waveforms (lower panels) of the 400-nm-thick film for each λ [Fig. 4(a) $\lambda = 1064$ nm, Fig. 4(b) 532 nm, Fig. 4(c) 355 nm, and Fig. 4(d) 266 nm]. Note that the waveforms are normalized by their peak values for clarity. At $\lambda = 1064$ and 532 nm, we see that both measured and simulated voltage waveforms are characterized well by a single exponential decay. In contrast, a clear difference between the two waveforms can be identified at $\lambda = 266$ and 355 nm, in which the measured voltages are characterized by a single-exponential decay, whereas the simulated voltages are characterized by a double-exponential decay.

To achieve further insights, the voltage waveforms in the thermal model were examined systematically for various d values of 5–600 nm. First, we note that the decay behavior of all the experimental voltage waveforms was expressed by a single-exponential decay $A\exp(-t/\tau)$ regardless of d (A, constant; τ, decay time). The simulated voltage waveforms also exhibited a single-exponential decay in the small d range, generally with $d < 200$ nm. However, as d increased, an additional fast decay component emerged and the decay was then expressed by a double-exponential function, $A_{\text{s}}\exp(-t/\tau_{\text{s}}) + A_{\text{f}}\exp(-t/\tau_{\text{f}})$. Here, A_{s} and A_{f} are constants, and τ_{s} and τ_{f} are the decay times of the original (or the slower) decay component and the additional fast decay component, respectively. Note that $A_{\text{f}} = 0$ gives conditions for films with small d, in which the voltage decay is expressed by a single-exponential function, $A_{\text{s}}\exp(-t/\tau_{\text{s}})$. The inset in Fig. 5 shows the ratio of the additional fast decay component to the entire simulated voltage signal $A_{\text{f}}/(A_{\text{s}} + A_{\text{f}})$ calculated for each λ. We see that the additional fast decay component in the simulation starts to develop at a smaller d for shorter λ and its portion to the entire voltage increases with increasing d. In this d range, the portion of A_{f} is negligible for $\lambda = 1064$ and 532 nm. Thus, the simulated waveforms of $d = 400$ nm at these two λ are characterized well by a single-exponential decay as shown in the lower panels in Figs. 4(a) and 4(b). In contrast, the portion of A_{f} becomes significant for $d > 250$ nm at $\lambda = 266$ and 355 nm. This is why a double-exponential decay behavior is clearly identified in the simulated waveforms of $d = 400$ nm at $\lambda = 355$ and 266 nm as shown in the lower panels in Figs. 4(c) and 4(d).

The emergence of the additional fast decay component in the simulation is qualitatively understandable from the following aspects. In general, thermal relaxation of a thin film grown on a substrate is governed by two mechanisms, that is, (i) heat diffusion within the film and (ii) heat transfer from the film to the substrate. Diffusion, which is related to the temperature gradient established inside the film, occurs so as to make the film temperature uniform, whereas heat transfer, which is related to the temperature drop at the film/substrate interface, occurs so as to remove excess heat from the film. For films with $d > 250$ nm, laser illumination at $\lambda = 266$ and 355 nm induces a large temperature increase at the air/film interface, but that at the film/substrate interface is negligible. This is due to the short optical penetration depth ($=\alpha^{-1}$) of the

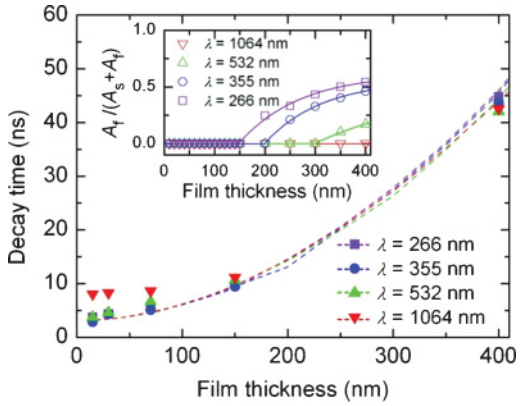

FIG. 5. (Color online) Film thickness d dependence of the voltage decay time for different λ. Filled symbols are experimental values, which are characterized by a single-exponential decay. Simulated voltage waveforms, in contrast, are characterized by a double-exponential decay, $A_s \exp(-t/\tau_s) + A_f \exp(-t/\tau_f)$, with a slower ($\tau_s$) and a faster ($\tau_f$) decay component. Here, only τ_s is shown, for clarity, by dashed lines. Note that τ_f appear only for $d > 200$ nm and are nearly d independent in this d range, with values of 6–8 ns. Inset: d dependence of $A_f/(A_s + A_f)$, which represents the ratio of the additional fast decay component to the entire voltage signal.

Ca_xCoO_2 films at these λ, which is about 75–110 nm. Under this situation, only heat diffusion contributes to the thermal relaxation in the first stage. The diffusion process gradually delivers the thermal energy to the film/substrate interface, which eventually increases the temperature at this region. This will now make heat transfer contribute to the thermal relaxation. The two relaxation mechanisms then proceed concurrently until the system reaches equilibrium. The double-exponential decay behavior that is observed in the thermal model for thick films clearly reflects the aforementioned two-stage process. Namely, τ_f reflects the thermal relaxation governed by only diffusion (the first-stage process), and τ_s reflects the thermal relaxation governed by simultaneous diffusion and transfer (the second-stage process, or the single process in films with small d).

From this point of view, the double-exponential decay in the simulated voltages is reasonable, and it seems rather odd that the additional fast decay does not emerge in the measured voltages (at $\lambda = 266$ and 355 nm in 400-nm-thick film). Nevertheless, we emphasize here that the decay time of the measured voltages τ_{meas} and that of the original (or the slower) decay of the simulated voltages τ_s show good agreement throughout the measured d range. Figure 5 shows d dependences of τ_{meas} (filled symbols) and τ_s (dashed lines) for different λ. The additional fast decay time τ_f in the simulation are not shown for clarity (τ_f were nearly d independent with fast values of 6–8 ns). In Fig. 5, one can clearly see that τ_{meas} and τ_s show the same d dependences and exhibit similar values. The good agreements between τ_{meas} and τ_s imply that the voltage decay is indeed related to thermal relaxation of the film. Yet, considering the issue regarding the additional fast decay, it seems that the ODTE effect alone is insufficient to fully explain the laser-induced voltage characteristics.

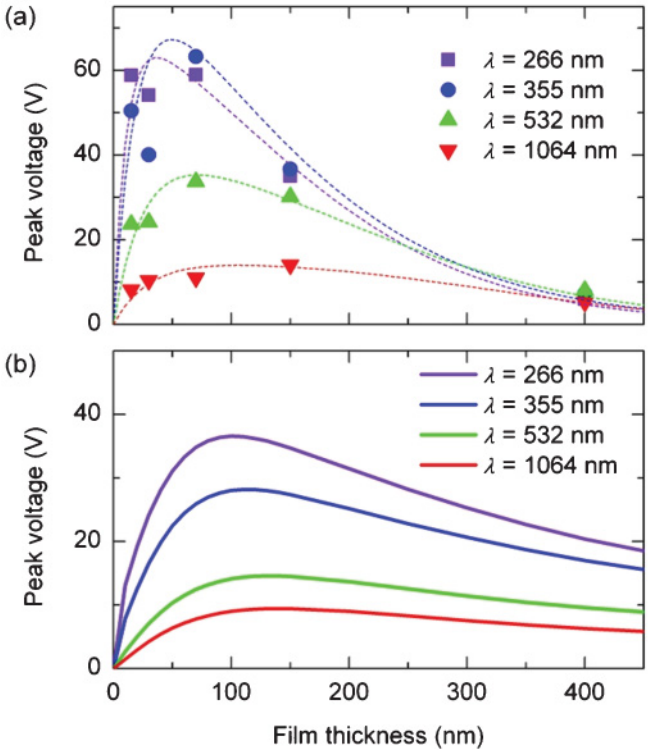

FIG. 6. (Color online) Film thickness dependence of the peak voltage: (a) experimental and (b) simulated by the thermal model. Dashed lines in (a) are a guide for the eye.

B. Peak voltage (amplitudes)

Figure 6(a) shows the measured V_{peak} as a function of d for each λ. At each λ, V_{peak} increases monotonically with decreasing d from 400 nm, but shows a maximum around 70 nm, and then decreases with further decreasing d. The magnitudes of V_{peak} at a fixed d tend to show higher values at shorter λ, except that little difference is identified between $\lambda = 355$ and 266 nm. In Fig. 6(b), we show d dependence of the simulated V_{peak} for each λ. The values of the simulated V_{peak} are of the same order of magnitude as those of the experiment. The slight difference in the magnitudes of V_{peak} in the experiment and the simulation may be related to the substituted physical quantities used in the simulation. A peak structure around $d = 70$ nm was also observed in the simulated $V_{peak}(d)$ curves. Meanwhile, we see two distinct features that are in contrast to the experiment. (i) The simulated V_{peak} values at $\lambda = 266$ nm are obviously larger than those at $\lambda = 355$ nm, whereas the measured V_{peak} values at these two λ are comparable. The simulation seems to be rather reasonable considering that more laser power is absorbed by the film at $\lambda = 266$ nm (thus larger $\nabla_z T$ and V_x). (ii) The simulated V_{peak} for $d = 400$ nm shows a considerable λ dependence, in contrast to the experiment, where it is independent of λ. The experimental V_{peak} values for $\lambda = 266$ and 355 nm are significantly suppressed relative to the simulated values.

The first discrepancy regarding V_{peak}, that is, the similar values in the measured V_{peak} at $\lambda = 266$ and 355 nm, can be understood by the suppression of ΔS due to laser heating. Based on the thermal model, laser illumination under the present condition introduces an increase in film temperature

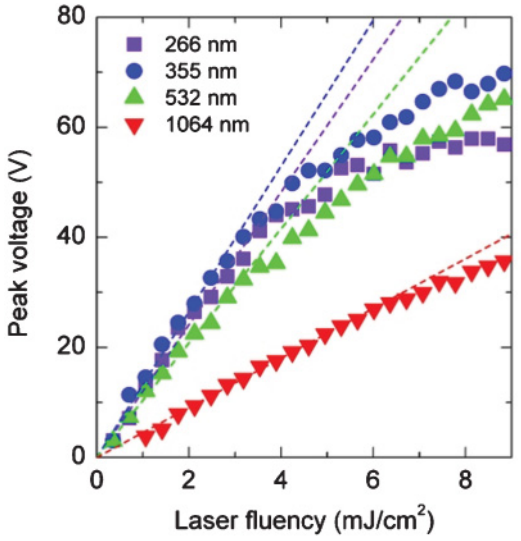

FIG. 7. (Color online) Laser fluency I dependence of the peak voltage of a 150-nm-thick Ca_xCoO_2 film measured at different λ values. Dashed lines represent linear fits to the data at each λ in the low-I range.

of up to several tens of kelvins. A temperature increase of this level will reduce the ΔS of the Ca_xCoO_2 film according to Ref. 13. In the present case, the reduction of ΔS by laser heating should be significant at shorter λ due to the increase in laser absorption. To achieve insights, we have measured the I dependence of V_{peak} of a 150 nm-thick Ca_xCoO_2 film. The results for each λ are shown in Fig. 7. For each λ, V_{peak} increases linearly with increasing I in the low-I range, which is consistent with the thermal model. However, with further increasing I, V_{peak} deviates from the linear response when its magnitude reaches 25–30 V. The deviation starts sooner (at lower I) for shorter λ. Here, the average temperature rise of the film at which the deviation starts is estimated to be around 30 ± 5 K for each λ. These aspects clearly manifest that excess laser heating suppresses ΔS and that it leads to suppression of V_{peak} relative to the simulated values. The suppression of ΔS is most significant at $\lambda = 266$ nm due to largest laser absorption. This makes the experimental V_{peak} values at $\lambda = 266$ nm close to those at $\lambda = 355$ nm as observed in Fig. 6(a).

Meanwhile, the above picture is insufficient to explain the second discrepancy regarding V_{peak}, that is, the λ independence in the measured V_{peak} for $d = 400$ nm. Indeed, suppression of ΔS by laser heating is significant at shorter λ and may lead to similar V_{peak} values between each λ, as explained above for the case at $\lambda = 266$ and 355 nm. However, the thermal model suggests that the average temperature rise of the film does not vary much for d of 70–400 nm. Therefore, suppression of ΔS at $\lambda = 266$ nm for the 70- and the 150-nm-thick films will be at the same level as that for the 400-nm-thick film. This means that λ independence of the V_{peak} is also expected for $d = 70$ and 150 nm from the aforementioned picture, which, however, is not the case in Fig. 6(a).

V. DISCUSSION

The discrepancies between the experiment and the thermal model, for both V_{peak} and τ, are significant at $\lambda = 266$ and 355 nm, that is, under the occurrence of interband transition. This suggests the presence of a photovoltaic contribution to the laser-induced voltage. To explain the discrepancies, here we propose the photo-Dember effect as a possible mechanism. The photo-Dember effect is one of the photovoltaic effects, which is associated with the diffusion of photoexcited electrons and holes.[18] It is often observed in common semiconductors[19,20] but is also reported in oxides.[21,22] For $E_{photon} > E_g$, laser illumination produces photoexcited carriers (electrons and holes) inside the material near the surface limited within the optical penetration depth. The photoexcited carriers generated near the surface then diffuse toward the other end of the material reflecting the carrier density gradient induced by laser illumination. Since electrons and holes usually exhibit different speeds of diffusion (mobility), the diffusion process leads to a macroscopic charge separation, which results in a transient photovoltaic signal (photo-Dember effect). We assume that this photo-Dember effect takes place in the Ca_xCoO_2 film at $\lambda = 266$ and 355 nm, where interband transition occurs. Although the mobility of electrons μ_e and holes μ_h are unknown for Ca_xCoO_2, an asymmetric energy band structure around the Fermi level, that is, a different dispersion between the valence band and the conduction band, has been reported in a related material, Sr_xCoO_2.[23] This feature in the energy diagram manifests a difference in the effective mass of electrons and holes, which indicates different values of μ_e and μ_h. Considering the close resemblance between the two materials, a similar energy diagram, thus difference in μ_e and μ_h, can also be expected for Ca_xCoO_2.

The photo-Dember field in Ca_xCoO_2 is expected to develop along the CoO_2 planes, in which carrier conduction is limited. In the tilted crystal orientation, the photoexcited carriers generated near the film surface will diffuse diagonally toward the film/substrate interface within the tilted CoO_2 planes. The schematic motion of the photoexcited carriers in the tilted Ca_xCoO_2 films is described in Fig. 8(a). Note that the sample dimension and the coordinates shown in Fig. 8(a) are the same as those in Fig. 1. Due to the diagonal motion of the photoexcited carriers, here we expect generation of a transverse voltage, which can be expressed as

$$V_{pD} = \frac{\Delta\phi_{pD}}{2}\frac{l}{d}\sin 2\theta. \tag{11}$$

Here, V_{pD} is the transverse photo-Dember voltage and $\Delta\phi_{pD}$ is the electric potential difference between the positions at the film surface and the film/substrate interface along a single CoO_2 plane [see Fig. 8(a)].

The temporal distribution of the photoexcited carriers can be calculated by a similar diffusion equation as that of the thermal model with a slight modification. Instead of D_T, we use D_e $(=k_BT\mu_e/q)$ and D_h $(=k_BT\mu_h/q)$, which are the diffusion coefficient of electrons and holes, respectively. Here, k_B and q are the Boltzmann constant and the elementary charge, respectively. For the boundary condition, R_{bd} is set to infinity, assuming that there is no carrier transfer at the film/substrate interface. The temporal profile of the photoexcited electron density ΔN_e and hole density ΔN_h

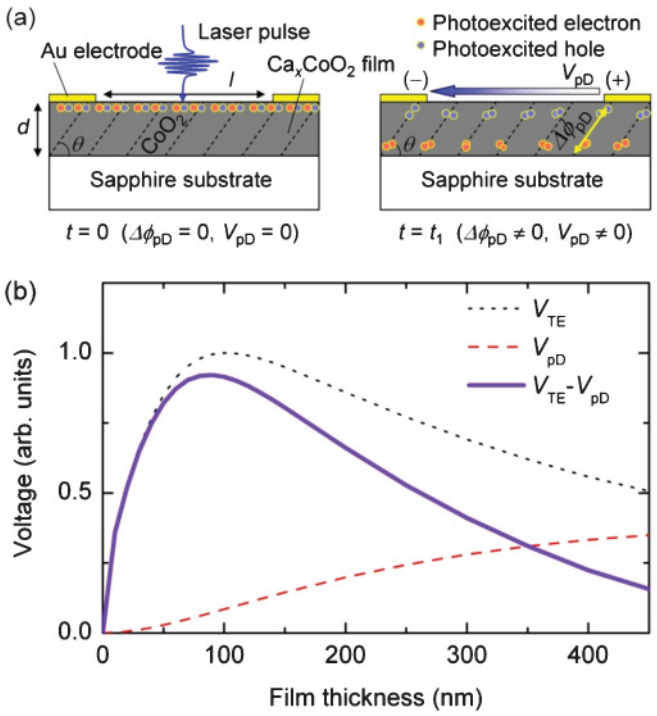

FIG. 8. (Color online) (a) Schematic cross section of a tilted Ca_xCoO_2 thin film, which describes the development of the transverse photo-Dember voltage. The left and right panels describe the condition immediately after laser illumination (at $t = 0$) and after a certain period of time (at $t = t_1$), respectively. Photoexcited carriers generated near the film surface are expected to diffuse diagonally along the tilted CoO_2 planes. (b) Simulated film thickness dependence of the ODTE voltage V_{TE} (dotted line), the photo-Dember voltage V_{pD} (dashed line), and the sum of V_{TE} and V_{pD} (solid line). Note that V_{TE} and V_{pD} have different polarities. See the polarity of V_x ($= V_{TE}$) depicted in Fig. 1.

will then be expressed as

$$\Delta N_e(z,t) = \sum_{n=1}^{\infty} N_n \cos\left(\frac{n\pi z}{d}\right) \exp\left(-D_e \frac{n^2\pi^2}{d^2} t\right), \quad (12)$$

$$\Delta N_h(z,t) = \sum_{n=1}^{\infty} N_n \cos\left(\frac{n\pi z}{d}\right) \exp\left(-D_h \frac{n^2\pi^2}{d^2} t\right). \quad (13)$$

Here, N_n is of the form

$$N_n = \frac{2}{d} \int_0^d N_i \cos\left(\frac{n\pi z}{d}\right) dz. \quad (14)$$

In this equation, N_i is the density of photoexcited carriers immediately after laser illumination, which is expressed as

$$N_i = \frac{I\alpha\lambda}{hc}(1 - R)\exp(-\alpha z), \quad (15)$$

where h is the Planck's constant and c is the speed of light. Using the spatial distribution of the photoexcited carriers in Eqs. (12) and (13), the electric potential ϕ distribution of the film can be calculated by solving the Poisson equation,

$$\frac{\partial^2\phi}{\partial z^2} = -\frac{\rho}{\epsilon}, \quad (16)$$

where ϵ is the dielectric constant and ρ is the charge density expressed by $q(\Delta N_h - \Delta N_e)$. $\Delta\phi_{pD}$ [$=\phi(0) - \phi(d)$] will then be expressed in the form

$$\Delta\phi_{pD} \propto \sum_{n=1}^{\infty} \frac{n^2\pi^2}{d^2} N_n\{1 - \cos(n\pi)\} \times \left\{\exp\left(-\frac{t}{\tau_e}\right) - \exp\left(-\frac{t}{\tau_h}\right)\right\}. \quad (17)$$

Here, τ_e and τ_h are given as $d^2/n^2\pi^2 D_e$ and $d^2/n^2\pi^2 D_h$, respectively. By substituting the right side of Eq. (17) into Eq. (11), the time development of the transverse photo-Dember voltage can be examined.

Since the values of μ_e and μ_h are unknown for Ca_xCoO_2, we examined the general features of the transverse photo-Dember voltage by assuming a condition of $\mu_e/\mu_h = 2$ (μ_e is larger than μ_h for the great majority of materials). We also assumed that the diffusion length of the photoexcited electrons and holes are larger than the d examined here because the diffusion length of indirect band gap materials generally exceeds several micrometers. The majority carriers in Ca_xCoO_2 are holes (a p-type material). For the configuration in Figs. 1 and 8(a), the polarity of the ODTE voltage between the electrodes will be positive in the left electrode and negative in the right electrode (see Fig. 1). In contrast, the polarity of the photo-Dember voltage will be opposite: positive in the right electrode and negative in the left electrode [see Fig. 8(a)]. This means that the ODTE field will be screened by the photo-Dember field when the two effects occur concurrently. In Fig. 8(b), we show d dependence of the calculated V_{pD} by the dashed lines. Note that the longitudinal axis in Fig. 8(b) is shown in arbitrary units. One can see that the magnitude of V_{pD} increases monotonically with increasing d. This indicates that the suppression of the ODTE voltage by the photo-Dember voltage becomes more significant in thicker films. The increase in the photo-Dember field with increasing d has also been observed experimentally in the previous report on terahertz radiation utilizing the photo-Dember effect.[24] In Fig. 8(b), we also show, by the dotted lines, the ODTE voltage V_{TE} at $\lambda = 266$ nm calculated by the thermal model. The measured V_{peak} signal should be the sum of V_{TE} and V_{pD}, which have opposite polarity, so $V_{peak} = V_{TE} - V_{pD}$. By adjusting the magnitude of V_{pD} to a certain level, the significant suppression of V_{peak} for thick films at $\lambda = 266$ and 355 nm, which is observed experimentally in Fig. 6(a) but not expected in the thermal model, can indeed be reproduced [see the solid line in Fig. 8(b)]. This explains the λ independence of the V_{peak} for $d = 400$ nm. We confirmed that the behavior of V_{pD} shown in Fig. 8(b) does not vary by the value of μ_e/μ_h, whether 2, 10, or 100. This indicates that the arbitrarily assumed μ_e/μ_h in the present simulation has no influence on qualitative discussion.

The duration of the transient photo-Dember voltage reported so far lies within a fast time scale, no more than several nanoseconds.[19,20,22] We therefore assume that the photo-Dember voltage in the Ca_xCoO_2 films will similarly show a fast time evolution. In the present situation, we expect the photo-Dember voltage to trace nearly the same time profile as does the laser pulse. This is because the laser pulse used here exhibits a pulse width of 8 ns, which is longer than the time scale of the previously reported photo-Dember voltages.

The lack of the additional fast decay component (τ_f of ~8 ns) in the measured voltage waveforms of the 400-nm-thick film is fairly reasonable if we consider that the photo-Dember effect, which is expected to occur within several nanoseconds, acts to screen this fast decay component of the ODTE field. In the thermal model, the portion of the fast decay component to the entire voltage in the 400-nm-thick film is estimated to be as large as one-half at $\lambda = 266$ nm (see the inset in Fig. 5). Thus, the measured voltage of the 400-nm-thick film at $\lambda = 266$ nm can be less than half the expected value without the fast decay component, that is, under the influence of the photo-Dember effect. A similar screening of the ODTE field by the photo-Dember field is also expected at $\lambda = 355$ nm. Although further analysis is necessary for quantitative understanding, we assume that the photo-Dember mechanism thus provides reasonable explanations for the discrepancies between the experiment and the thermal model in both V_{peak} and τ.

VI. SUMMARY

The laser-induced voltage characteristics in tilted Ca_xCoO_2 thin films were investigated using a Nd:YAG pulse laser at various λ. The thermal model based on the heat conduction equation provided a good explanation for the laser-induced voltages originating mainly from the ODTE effect. However, we identified several signatures, which were different from the thermal model when the laser illumination was accompanied by interband transition. We demonstrated that these discrepancies can be understood qualitatively by taking account of the photo-Dember effect. The influence of photovoltaic effect on the laser-induced voltages in tilted thin films has been debated ever since the discovery of this phenomenon in $YBa_2Cu_3O_{7-\delta}$ thin films. Our result suggests that the laser-induced voltage is purely thermal in origin when $E_{photon} < E_g$ but is affected by a photovoltaic contribution when $E_{photon} > E_g$.

*takahashi.kohei@jp.panasonic.com

[1] H. Lengfellner, G. Kremb, A. Schnellbögl, J. Betz, K. F. Renk, and W. Prettl, Appl. Phys. Lett. **60**, 501 (1992).

[2] H. Lengfellner, S. Zeuner, W. Prettl, and K. F. Renka, Europhys. Lett. **25**, 375 (1994).

[3] S. Zeuner, H. Lengfellner, and W. Prettl, Phys. Rev. B **51**, 11903 (1995).

[4] S. Zeuner, W. Prettl, and H. Lengfellner, Appl. Phys. Lett. **66**, 1833 (1995).

[5] Th. Zahner, R. Stierstorfer, S. Reindl, T. Schauer, A. Penzkofer, and H. Lengfellner, Physica C **313**, 37 (1999).

[6] X. H. Li, H.-U. Habermeier, and P. X. Zhang, J. Magn. Magn. Mater. **211**, 232 (2000).

[7] H.-U. Habermeier, X. H. Li, P. X. Zhang, and B. Leibold, Solid State Commun. **110**, 473 (1999).

[8] K. Zhao, K.-J. Jin, Y.-H. Huang, H.-B. Lu, M. He, Z.-H. Chen, Y.-L. Zhou, and G.-Z. Yang, Physica B **373**, 72 (2006).

[9] K. Takahashi, T. Kanno, A. Sakai, H. Adachi, and Y. Yamada, Appl. Phys. Lett. **97**, 021906 (2010).

[10] B. L. Cushing and J. B. Wiley, J. Solid State Chem. **141**, 385 (1998).

[11] K. Takahashi, A. Sakai, H. Adachi, and T. Kanno, J. Phys. D Appl. Phys. **43**, 165403 (2010).

[12] H. S. Kwok and J. P. Zheng, Phys. Rev. B **46**, 3692 (1992).

[13] T. Kanno, S. Yotsuhashi, and H. Adachi, Appl. Phys. Lett. **85**, 739 (2004).

[14] K. Takahashi, A. Sakai, T. Kanno, and H. Adachi, Appl. Phys. Lett. **95**, 051913 (2009).

[15] S. Zeuner, H. Lengfellner, J. Betz, K. F. Renk, and W. Prettl, Appl. Phys. Lett. **61**, 973 (1992).

[16] A. Satake, H. Tanaka, T. Ohkawa, T. Fujii, and I. Terasaki, J. Appl. Phys. **96**, 931 (2004).

[17] A. Zorkovská, M. Orendáč, J. Šebek, E. Šantavá, P. Svoboda, I. Bradarić, I. Savić, and A. Feher, Phys. Rev. B **72**, 132412 (2005).

[18] K. Seeger, *Semiconductor Physics: An Introduction*, 9th ed. (Springer, Berlin, 2004), pp. 151–152.

[19] P. Gu, M. Tani, S. Kono, K. Sakai, and X.-C. Zhang, J. Appl. Phys. **91**, 5533 (2002).

[20] K. Liu, J. Xu, T. Yuan, and X.-C. Zhang, Phys. Rev. B **73**, 155330 (2006).

[21] K.-J. Jin, K. Zhao, H.-B. Lu, L. Liao, and G.-Z. Yang, Appl. Phys. Lett. **91**, 081906 (2007).

[22] K.-J. Jin, H.-B. Lu, K. Zhao, C. Ge, M. He, and G.-Z. Yang, Adv. Mater. **21**, 4636 (2009).

[23] R. J. Xiao, H. X. Yang, L. F. Xu, H. R. Zhang, Y. G. Shi, and J. Q. Li, Solid State Commun. **135**, 687 (2005).

[24] C. T. Que, T. Edamura, M. Nakajima, M. Tani, and M. Hangyo, Jpn. J. Appl. Phys. **48**, 010211 (2009).